Evaluation of Vibration-Based Health Assessment and Diagnostic Techniques for Helicopter Bearing Components

David Siegel [1], Canh Ly [2], Jay Lee [1]

[1] *Center for Intelligent Maintenance Systems, University of Cincinnati, P.O Box 210072, Cincinnati, OH 45221-0072, United States*
[2] *Army Research Lab - SEDD, 2800 Powder Mill Road, Adelphi, MD 20783, United States*

Abstract

Improved techniques for estimating the level of degradation on helicopter drive-train components can provide a substantial benefit with regards to improved safety and maintenance cost reduction. This study focuses on the oil-cooler bearing, which is a key component on the rotorcraft. Vibration data from an oil-cooler bearing test-rig provided by Impact Technologies, LLC. consisted of both baseline and run-to-failure data sets collected under different loading and speed regimes. A multitude of feature extraction methods were used, including time domain features, frequency domain features, envelope features, and others. A self-organizing map, multi-feature distance metric is used to quantify the health of the bearing in each operating regime. The health assessment results for the two run-to-failure data sets show promising results, in that there is a noticeable degradation trend and a similar end-health value is reached. Future work will consider developing remaining life prediction techniques, including regression-based methods and Bayesian filtering techniques.

Keywords: Bearing Health Assessment**,** Self-Organizing Map, Bearing Envelope Analysis, Bearing Fault Progression

1. Introduction

The shift towards a condition-based maintenance approach and, in particular, for rotorcraft drive train components, has the potential to provide a substantial benefit with regards to reliability, availability, safety, and maintainability. However, these potential benefits can only be realized if the helicopter health and usage monitoring systems can provide robust identification of the fault type and severity [1]. Although vibration diagnostic systems are currently used to monitor helicopter fleets, enhanced methods for extracting more discriminatory vibration indicators, or using machine-learning algorithms to estimate the health, could provide a more accurate health monitoring system. Considering the amount of rotorcraft drive components, and each component having potentially multiple failure modes, the scope for improving current diagnostic capabilities is usually limited to a few key critical components. This particular study was focused on the oil-cooler bearing, in which the leading cause of failure seen in the field was due to corrosion. The aim of this research was to develop a technique to estimate the bearing condition over time as the damage progressed into a localized spall on the bearing raceways and eventual failure.

Techniques for monitoring the condition of a bearing with localized spall damage consist of many methods, with the most traditional including the use of statistical time domain

features, such as the root mean square, peak to peak, kurtosis, and crest factor [2]. The use of the vibration spectrum and the bearing fault frequencies is also common; however, in many instances, the bearing fault frequency peaks in the vibration spectrum are close to the noise floor during the incipient stages of bearing damage [3]. One of the more popular techniques is the use of the high frequency envelope method, also referred to as bearing envelope analysis. Demodulating of a specific high frequency band and extracting energy from the envelope spectrum at the bearing fault frequencies have shown to be more effective than the traditional Fast Fourier Transform (FFT) spectrum [4]. Other studies have evaluated time-frequency representations of the vibration signal to characterize the transient nature of the impact created by a localized spall; these techniques include the use of the short time Fourier transform, the Wigner Ville distribution, the continuous wavelet transform, and the Hilbert-Huang Transform [5-6]. In more recent work, features extracted from the intrinsic mode functions after performing the empirical mode decomposition of the vibration signals have shown promise, and the ability to discriminate between a good and a degraded bearing condition [7].

Although there is much prior work on understanding the vibration signature of bearings with localized spall damage, many of those studies consisted of seeded faults, in which the bearings were induced with discrete levels of damage. The results with induced levels of discrete spall damage can be considered snapshots of the bearing condition over time, and understanding the various vibration indicators as the damage progresses until failure can provide a more indicative story of the relative merits of the vibration indicators. It is not uncommon in diagnosis of mechanical drive-train systems to have vibration indicators that are only suitable for detecting incipient degradation but do not trend well over time; various studies related to developing vibration based indicators for gear components have discussed this aspect [8]. By evaluating the various signal processing and feature extraction methods with run-to-failure data sets, the features can be examined in terms of both their ability to detect incipient damage, as well as their ability to trend with the progression of the bearing degradation. The progression of the bearing degradation until a failure point might not be characterized by a single vibration indicator, and this study also evaluates a multi-feature based health assessment method.

The organization of the paper consists of an overview of the experimental setup and data acquisition in section 2, followed by a discussion of the signal processing methods used to process the vibration signals in section 3. Section 4 includes the method and results for characterizing the bearing health over time. Conclusions and suggestions for future work are provided in section 5.

2. Experimental Setup and Data Acquisition

In order to facilitate an understanding of the vibration response with respect to describing the bearing health from no visual damage to spalling and eventual failure, an oil-cooler bearing test-rig stand was constructed by Impact Technologies LLC. The test-rig is shown in Fig. 1 and consists of a radial and axial accelerometer, a load cell to measure the axial load, pneumatic regulators to monitor the radial load, thermocouples attached on the bearing raceways, and a tachometer signal to provide a measure of the shaft speed. Data was acquired using a National Instruments-based PXI system, and the vibration data was sampled at a rate of 102.4 KHz. Each data file consisted of 102,400 samples, which

provided a sampling time of 1 s for each data file and a frequency resolution of 1Hz for spectrum analysis.

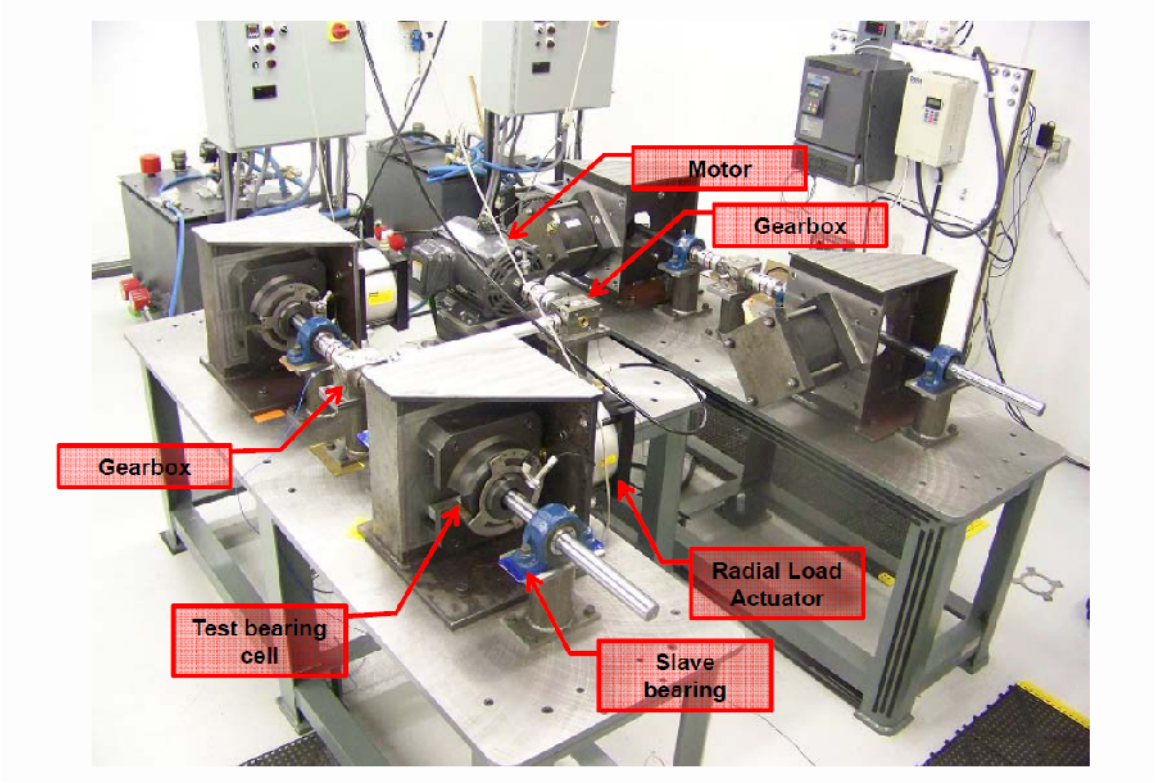


Fig. 1: Oil-Cooler Bearing Test-Rig (Photo from Impact Technologies, LLC.)

In order to abbreviate the time required to initiate localized damage on the bearing races, bearings with different corrosion levels are used in the run-to-failure testing. This would also simulate a potential scenario in the field in which a corroded bearing could potentially develop a localized spall with increased usage. The bearing run-to-failure test procedure used a bearing with a specified corrosion level and conditioned the bearing to different loading conditions until the eventual failure of the rolling element bearing. The run-to-failure testing resulted in the inner race failure of two bearings; the data sets for these two bearings were the ones used to evaluate the proposed health assessment techniques. The loading profile for these two run-to-failure data sets is shown in Fig. 2. The loading profile illustrates that the radial loading was only applied after the shaft reached a rotational speed of 75Hz; this was the predominant shaft speed at which the test was conducted. However, the radial load was stepped up or down to different increments in efforts to accelerate the initial time to reach an incipient level of damage, or to provide a reduced load during the progression of the bearing spall. These two bearings were inspected at various times, and information was documented when spall initiation took place and also at other intervals during the testing. Considering that the bearing was operated under different loading conditions, the proposed health assessment method would require a health model for each operating regime; section 4 discusses this aspect in more detail.

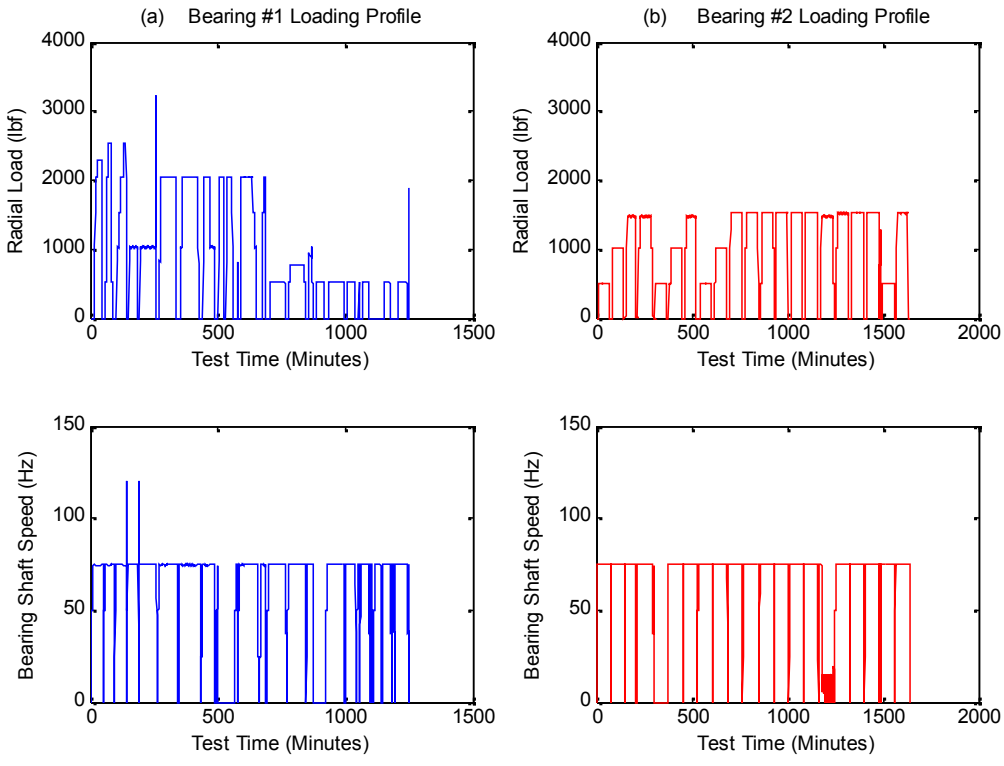


Fig. 2: Bearing Run-To-Failure Loading Profile, (a) Bearing #1, (b) Bearing #2

3. Signal Processing and Feature Extraction Methods

For developing vibration-based diagnostic and health assessment methods, the signal processing and feature extraction methods can be considered the foundation. Regardless of the classification, machine-learning, or prediction algorithms that are used, they almost universally require vibration indicators that are correlated with degradation of the mechanical system. Considering the overall importance of using the proper signal processing techniques, it is important to review the relevant methods and the merits of each potential method that was considered for this study. The techniques presented range from traditional time and frequency domain methods, to more sophisticated methods such as the high frequency envelope method and time synchronous averaging. The example plots are shown for Bearing #2 as a means of highlighting the processing techniques. However, the same processing methods were also applied to the other run-to-failure data set, and the feature trends and health results are presented for both data sets in section 4.

3.1 Time Domain

Extracting statistical features from the vibration time waveform can provide an indication of the overall condition of the monitored mechanical system, although its ability for providing fault identification is limited. The reason for the limited root cause information is that any change in a mechanical system, such as imbalance in a shaft, pitting of a gear tooth, shaft misalignment, or a damaged inner race of a bearing, would result in a noticeable change in the vibration level and the statistical indicators extracted from the vibration signal [9]. The root mean square is one of the more common vibration features extracted from the time signal and is shown in Eqn 1, in which x_i is the measured signal and N is the number of samples in the measured signal. The kurtosis indicator is another

commonly used vibration feature that is a statistical measure of the distribution of the vibration signal; for a mechanical system without defect, the expected kurtosis value would be approximately 3, and a degraded system would deviate from this value. The mathematical formulation for the kurtosis value is provided in Eqn 2, in which $\bar{x}$ is the mean and σ is the standard deviation of the measured signal [10]. Other time indicators included in this particular study include the crest factor, peak-to-peak, and the variance; however, this is not an exhaustive list of all potential time domain features that have been used in the literature.

$$RMS = \sqrt{\frac{1}{N}\sum_{i=1}^{N} x_i^{\,2}} \tag{1}$$

$$Kurtosis = \frac{\frac{1}{N}\sum_{i=1}^{N}(x_i - \bar{x})^4}{\sigma^4} \tag{2}$$

An example time waveform from the bearing at the start of the progression test, and also during the initiation of a spall on the bearing inner race, is presented in Fig. 3. The bearing with an inner race spall clearly has a higher amount of vibration energy; extracting the peak-to-peak or root mean square (RMS) of the waveform should describe this higher vibration level. Whether other potential techniques can provide more discrimination between the healthy and degraded state or a better degradation trend over time is the motivation for evaluating multiple techniques.

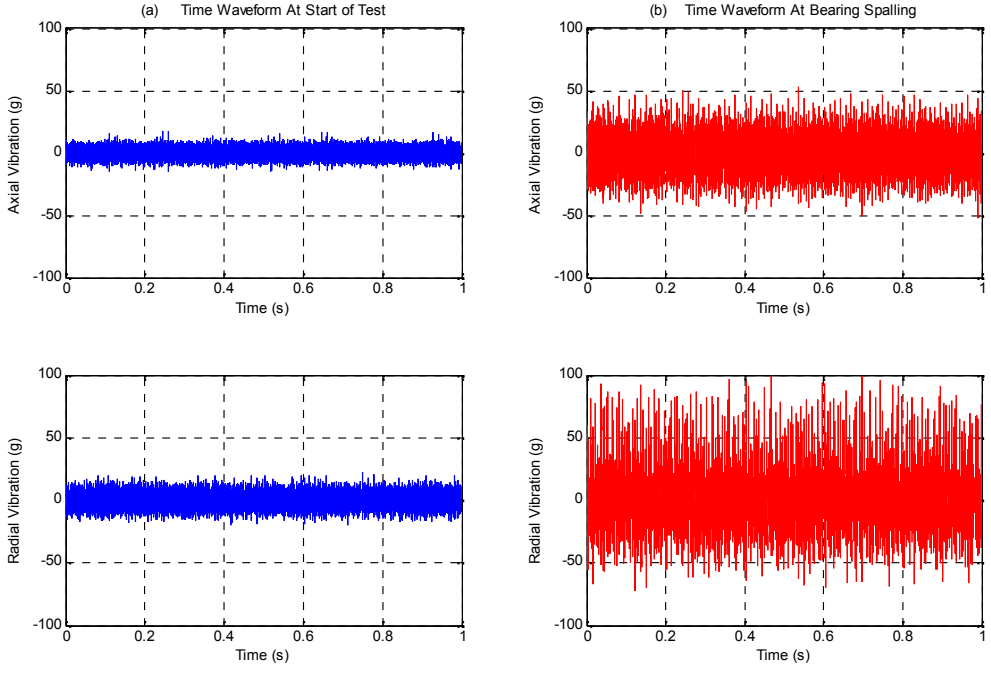


Fig. 3: Vibration Waveform,
(a) At the Start of Test, (b) With Early Stages of Inner Race Spall

3.2 Frequency Domain

The FFT and extracting information from the vibration spectrum is a classical technique that has been used for assessing the health of mechanical systems. As a reference, the

discrete form of the Fourier Transform is provided in Eqn 3, in which x_i is the measured signal in discrete form, X(k) is the frequency spectrum, N is the number of samples, and i and k are indices for the time and frequency domain signal, respectively. A discussion of the discrete Fourier Transform properties and potential errors, such as leakage, can be found in other references [11-12]. For the purpose of mechanical diagnosis, the key requirements would be that the signal is stationary and also that there is sufficient frequency resolution to isolate particular frequency bands of interest related to different faults.

$$X(k) = \frac{1}{N}\sum_{i=0}^{N-1} x_i \exp(-j2\pi ki/N) \tag{3}$$

For rolling element bearings, there are specific frequencies related to damage at a particular location on the bearing, such as the inner or outer race; these specific frequencies are called the bearing fault frequencies and are based on known kinematic relationships. The bearing fault frequency equations are listed in Eqn 4-8; the BPFI, BPFO, BSF, and FTF are called the ball pass frequency inner race, the ball pass frequency outer race, the ball spin frequency, and the fault train frequency, respectively. The parameters used to calculate the bearing fault frequencies are based on the bearing shaft speed (f) and geometric parameters, which include the following: the number of rolling elements, N_b; P_d, which is the pitch diameter; B_d, the ball diameter; and the contact angle, θ [13].

$$BPFI = \frac{N_b}{2} * f\left[1 + \left(\frac{B_d}{P_d}\right)\cos\theta\right] \tag{4}$$

$$BPFO = \frac{N_b}{2} * f\left[1 - \left(\frac{B_d}{P_d}\right)\cos\theta\right] \tag{5}$$

$$BSF = \left(\frac{P_d}{2 * B_d}\right) * f\left[1 - \left(\left(\frac{B_d}{P_d}\right)\cos\theta\right)^2\right] \tag{6}$$

$$FTF = \frac{f}{2}\left[1 - \left(\frac{B_d}{P_d}\right)\cos\theta\right] \tag{7}$$

$$\text{Rolling Element Defect Frequency} = 2 * \text{BSF} \tag{8}$$

For the oil-cooler helicopter bearing used in the test-rig, the geometric parameters are listed in Table 1. Using equations 4-8 and a shaft speed of 75 Hz, the bearing fault frequencies for this specific bearing can be calculated in a straightforward manner and are shown in Table 2. The calculated fault frequencies and the ones observed in the frequency spectrum might differ by a few Hertz; this is because the bearing fault frequency equations are based on the kinematic assumption of no slip, which is never perfectly achieved in a real system.

Table 1: Oil Cooler Bearing Geometry Parameters

Bearing Geometry Parameter	
# of Rolling Elements	10
Ball Diameter (mm)	12.7
Pitch Diameter (mm)	70
Contant Angle (radian)	0

Table 2: Calculated Bearing Fault Frequencies

Bearing Fault Frequency Name	Order	Frequency (Hz)
BPFI	5.91	443.04
BPFO	4.09	306.96
BSF	2.67	199.89
FTF	0.41	30.70
Rolling Element	5.33	399.78

The frequency spectrum can often highlight various forms of information. The broadband spectrum shown in Fig. 4 clearly illustrates that there is much more vibration energy in the 3000-16,000 Hz region for the bearing, with the early stages of spall damage compared with a bearing at the start of the run-to-failure testing. The higher vibration energy in this frequency band is likely due to some of the bearing modal frequencies being excited by the impact cause by a localized spall. Techniques to extract information from this aspect are discussed in more detail in the section pertaining to the bearing envelope analysis method.

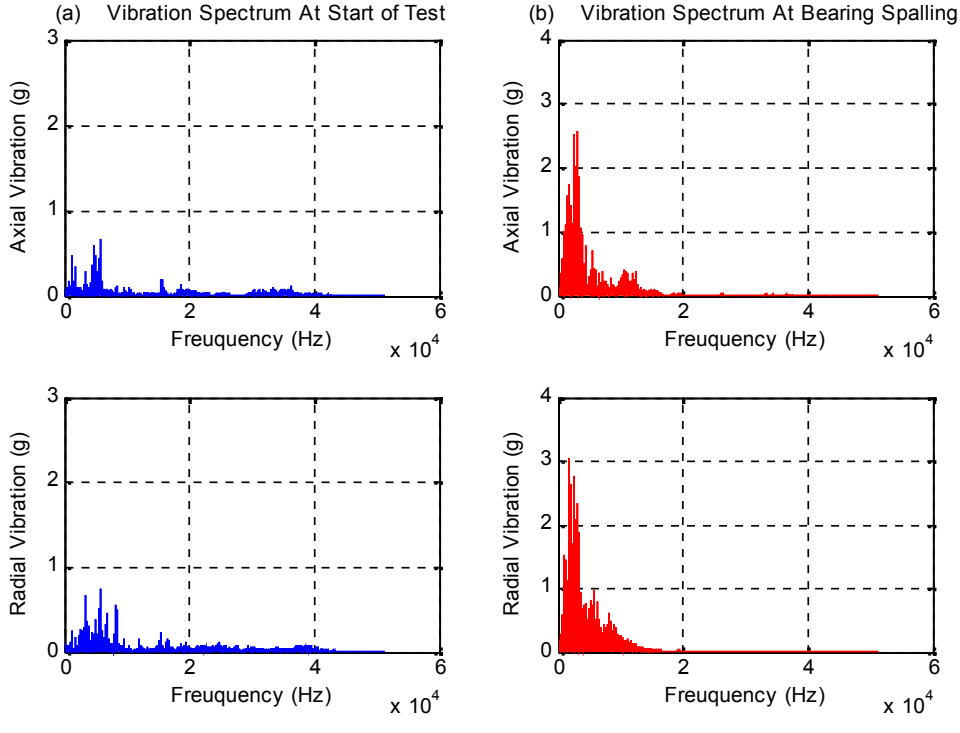


Fig. 4: Broadband Frequency Spectrum
(a) At the Start of Test, (b) With Early Stages of Inner Race Spall

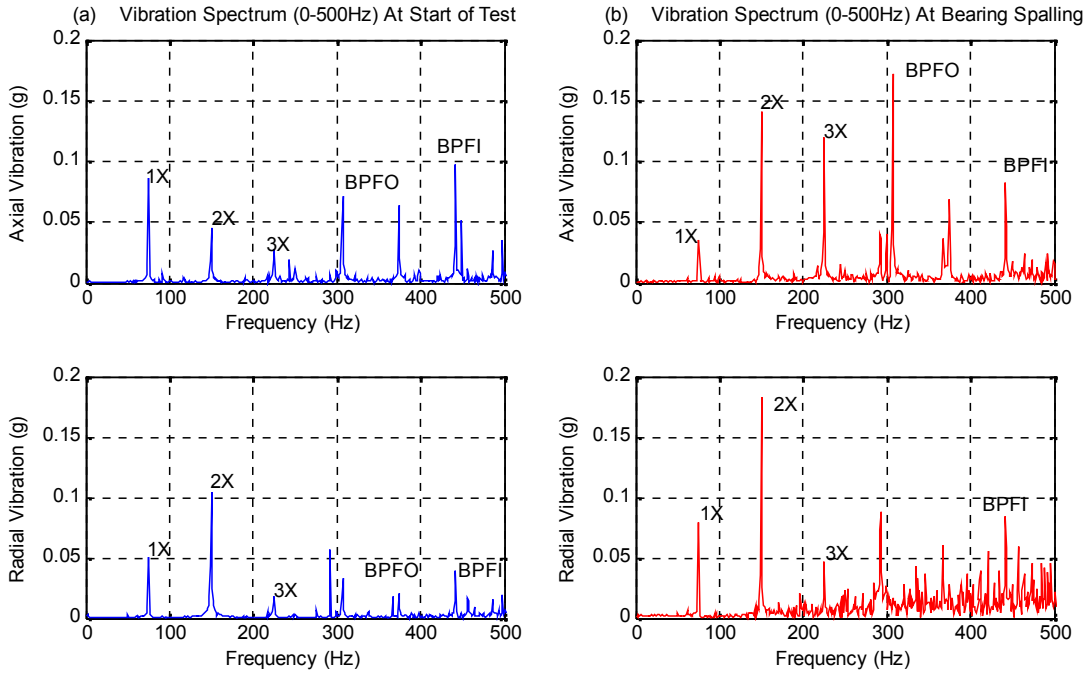


Fig. 5: Frequency Spectrum 0-500Hz
(a) At the Start of Test, (b) With Early Stages of Inner Race Spall

The bearing fault frequencies are in a much lower frequency range, with the ball pass frequency inner race occurring at 443 Hz and the other fault frequencies at a frequency below the BPFI. Fig. 5 highlights the vibration spectrum in the frequency range of 0-500 Hz for a bearing at the start of the test and one in which a spall was observed. Peaks related to shaft harmonics, as well as the bearing fault frequencies, can be clearly identified in this frequency band of interest. Even with the bearing at the start of the test, the bearing fault frequency peaks can be observed. However, whether these particular peaks showed an increasing trend with time would be more indicative of the merits of condition indicators based on the FFT fault frequencies.

3.3 Bearing Envelope Analysis

Prior to discussing the mathematical equations used to perform the bearing envelope analysis method, it is perhaps more intuitive to start with a high-level flow chat shown in Fig. 6. The bearing envelope analysis method consists of first selecting an appropriate band-pass filter around an excited natural frequency. The selection of the band-pass frequency band is actually one of the most critical and debated steps in this method, as selection of the band can have a large influence on the results of using the envelope method. However, the criteria for selecting the appropriate band is a research subject, and different techniques include the use of modal analysis, looking at kurtosis values in certain frequency bands (spectral kurtosis), and figures of merit, which include the ability to provide indicators that trend over time [14-15]. Comparing spectrums was used for selecting the appropriate band for this study; developing improved methods for band-pass filter selection likely requires a focused study on that topic alone and is beyond the scope of this work. A Chebyshev third order band-pass filter for this study was used and centered at 15,000 Hz, with upper and lower bounds of 14,100Hz and 15,900Hz respectively.

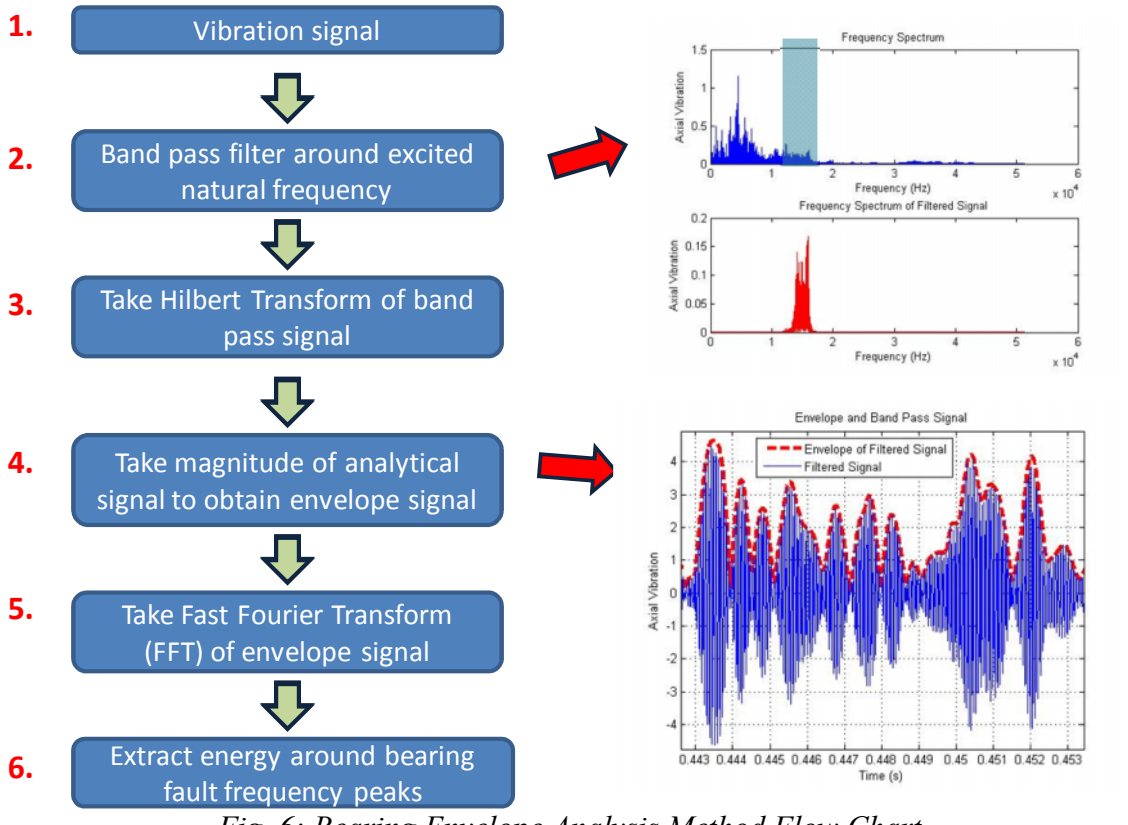


Fig. 6: Bearing Envelope Analysis Method Flow Chart

Prior to discussing the second step, which is taking the Hilbert Transform of the band-pass filtered signal; it is important to highlight the physical basis for why this particular transform is used. When a localized bearing spall is induced on the bearing, such as the inner race, it creates impulses that excite a few high frequency modes of the system. At this high frequency band, there is amplitude modulation, in which the carrier signal is associated with the excited resonance, and the low frequency modulating signal contains frequencies related to the bearing fault frequencies and is the signal of interest. Mathematical representations of amplitude modulation are provided in Eqn 9 and Eqn 10, in which f_c is the carrier frequency, f_m is the modulation frequency, β is the modulation index, and A is the modulated amplitude of the signal [3].

$$x(t) = A * \cos(2\pi * f_c * t) \tag{9}$$

$$A = A_o\left(1 + \beta * \cos(2\pi * f_m * t)\right) \tag{10}$$

The Hilbert Transform is used to demodulate the amplitude-modulated band-pass signal and extract the envelope signal, which contains low frequency information related to the bearing fault frequency repetitive impacts. The Hilbert Transform is shown in Eqn 11 and is a convolution operation between $1/(\pi t)$ and the measured signal x(t), with P being the Cauchy principal value [16]. For this application, x(t) would be the band-pass signal and not the original broadband signal.

$$y(t) = \frac{1}{\pi} P \int_{-\infty}^{\infty} \frac{x(\tau)}{t - \tau} d\tau \tag{11}$$

The signal after performing the Hilbert Transform y(t) forms a complex conjugate pair with the original signal x(t); a representation of these conjugate pairs is provided in Eqn 12, in which z(t) is called the analytical signal. By taking the magnitude of the analytical signal, the resultant signal is the envelope signal, as shown in the overall flow chart provided in Fig. 6.

$$z(t) = x(t) + j * y(t) \tag{12}$$

The remaining steps include performing a Fast Fourier Transform operation on the envelope signal and extracting energy around the calculated bearing fault frequencies. The resultant spectrum from this series of processes is commonly titled the envelope spectrum [4]. The envelope spectrum is plotted in Fig. 7 for a bearing in a good condition at the start of the test and for the same bearing later on in the test when it had early stages of spall damage. The peak related to the inner race fault (BPFI) is much more noticeable in the bearing with inner race damage compared to the bearing at the start of the test. The ratio in magnitude of the BPFI peak for the spalled and normal bearing at this particular snapshot is four, indicating that there is some separation in this condition indicator between a good and damaged bearing.

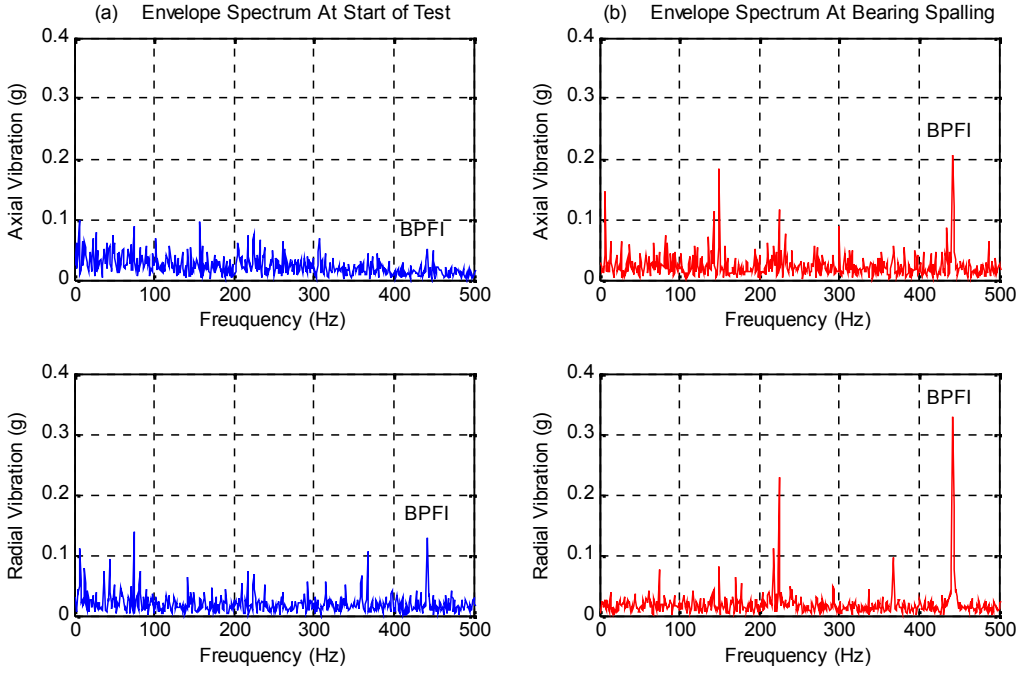


Fig. 7: Envelope Spectrum,
(a) At the Start of Test, (b) With Early Stages of Inner Race Spall

3.4 Time Synchronous Averaging

The time synchronous average is a common technique for processing vibration data related to systems with gear components, in that many frequencies of interest related to gear faults are synchronous with the shaft [17]. For monitoring the condition of rolling element bearing components, the fault frequencies are usually non-synchronous with the shaft speed, reducing the effectiveness of synchronous averaging [18]. However, whether any particular harmonics in the shaft increased due to moderate to high levels of bearing damage was worth exploring, and, thus, it was worthwhile to carry out the synchronous

averaging method for this application. Also, a residual signal is calculated that removes the DC component and the first 10 shaft harmonics; various time domain features can be also be processed on the residual signal.

The requirements for synchronous averaging include a tachometer signal and a vibration signal. The tachometer signal provides a pulse train that is indicative of the rotational speed of the shaft and is used to resample the vibration data into evenly space angular samples. After aligning the vibration signal into blocks of data that are some multiple of the shaft rotation, each block is added and then divided by the number of sample blocks to provide the synchronous averaged signal. This essentially highlights the vibration that is synchronous with the shaft and averages out the random or noise component of the signal [19]. There are analogous expressions based on Shannon's Sampling theorem and the Rayleigh criterion for order resolution and maximum order of interest, in that the order resolution is determined by the number of revolutions contained in the averaged sample, and the maximum order of interest is determined by the number of samples per angular rotation [20]. For example, a time synchronous averaged signal that contains 10 revolutions would provide an order resolution of 0.1; in an analogous manner, a time waveform that is acquired for 10 s would have a frequency resolution of 0.1Hz.

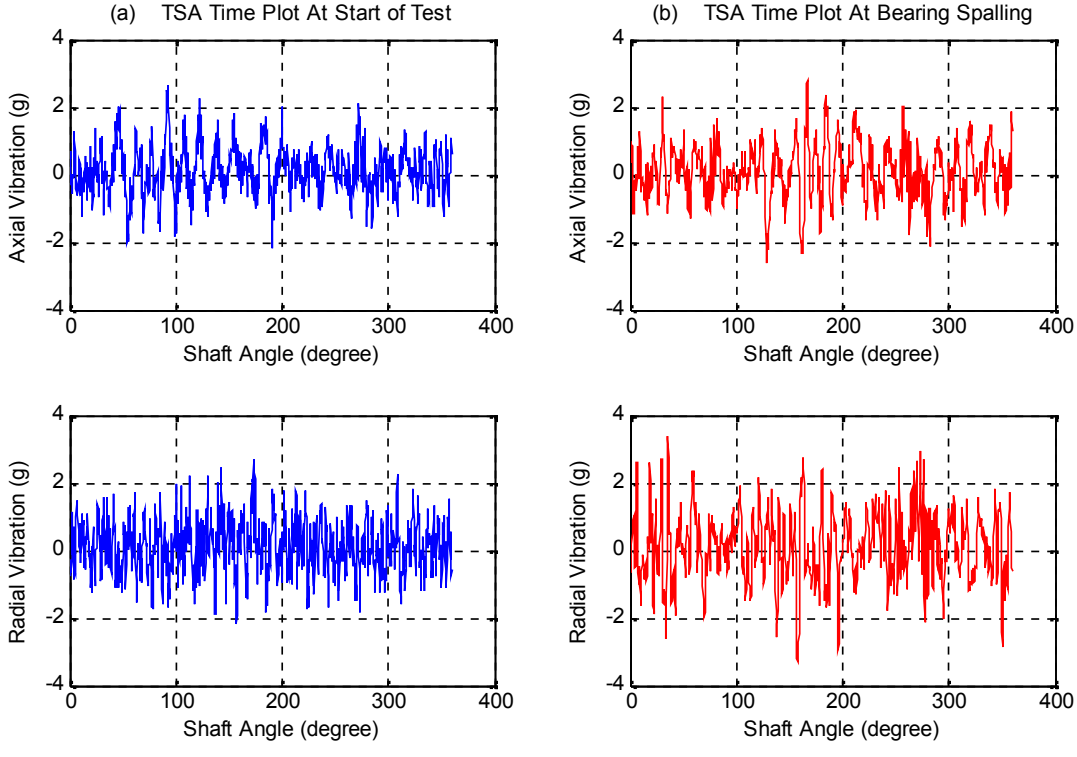


Fig. 8: Time Synchronous Average Signal
(a) At the Start of Test, (b) With Early Stages of Inner Race Spall

An example tine synchronous average signal is shown for a bearing in a healthy state at the beginning of the test and a bearing with an inner race spall in Fig. 8. From this particular plot of the time synchronous average, there is not any clear visual difference between the two signatures. However, whether any indicators in the time synchronous average waveform, the time synchronous average spectrum, or the residual signal provide a trend over time is investigated further during the feature selection process.

3.5 Spectral Kurtosis

The use of spectral kurtosis and methods related to this particular method, such as the kurtogram, were first used for diagnosis of mechanical systems by Antoni and Randall [21-22]. This processing method has two potential usages—one in the selection of an appropriate frequency band for applying the bearing envelope method, and also for machine surveillance. With regards to machine surveillance, this particular term is referring to monitoring the overall condition of the machinery, as opposed to specific processing techniques that provide root cause information on the particular fault that is occurring. For this application, its usage was related to machine surveillance, in that indicators from the spectral kurtosis information were evaluated with regards to whether they provided a noticeable degradation trend over the time from initial bearing spall to failure.

The spectral kurtosis calculation consists of first performing a Short Time Fourier Transform (STFT) on the vibration signal. Selecting the appropriate block size for performing the STFT in this method is a research topic; for this application, however, a few comparison plots of performing this calculation showed that a block size of 1024 provided acceptable results [22]. After performing the STFT, a kurtosis calculation is done at each frequency line. This provides a kurtosis value that is a function of frequency, and the given resolution of the kurtosis value is determined by the STFT block size and the number of samples in the processed data. For extracting features from this kurtosis indicator defined across the frequency spectrum, summing the kurtosis values in 5 equally spaced bands was the method used for this particular study. Other metrics from the spectral kurtosis, such as the maximum kurtosis value in a certain frequency band, could be considered, as well.

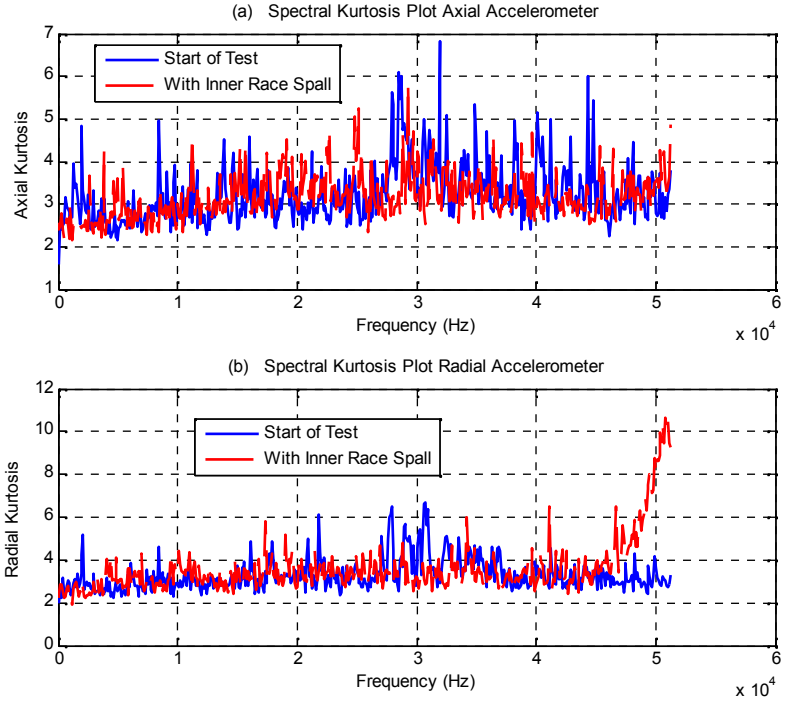


Fig. 9: Spectral Kurtosis Plot, (a) Axial Accelerometer, (b) Radial Accelerometer

An example plot of the spectral kurtosis is provided in Fig. 9, in which example data files consisted of the same bearing at the start of the test and when a spall was observed on the

inner race. From a visual standpoint, there is some difference between the kurtosis values in a high frequency band for the radial accelerometer, although this is not seen for the axial accelerometer. The true measure would be whether this difference is seen with the other data files during the failure progression, and also whether the features extracted from this method show a consistent trend over time.

4. Bearing Health Assessment Method and Results

4.1 Failure Progression and Feature Trends

Considering the multitude of features that were extracted from the vibratory data, presenting the trend in each individual feature over time as the bearing progressed to failure is not feasible; instead, a select subset of feature trends are presented to highlight some of the key observations. Given that the bearing was operated under different loading conditions, the feature trend results are presented in the operating regime that was most prevalent during the run-to-failure test. As the bearing spall worsens, one would expect the overall vibration level and the statistical properties of the vibration to change or experience an increase. The trends in the axial vibration RMS and peak-to-peak are presented in Fig. 10 for both bearings; notice in particular the clear increasing trend seen for Bearing #2 in the RMS and peak–to-peak feature. The trend observed for these same set of features for Bearing #1 shows a less gradual progression over time; however, there is a clear difference in magnitude at the end of the test.

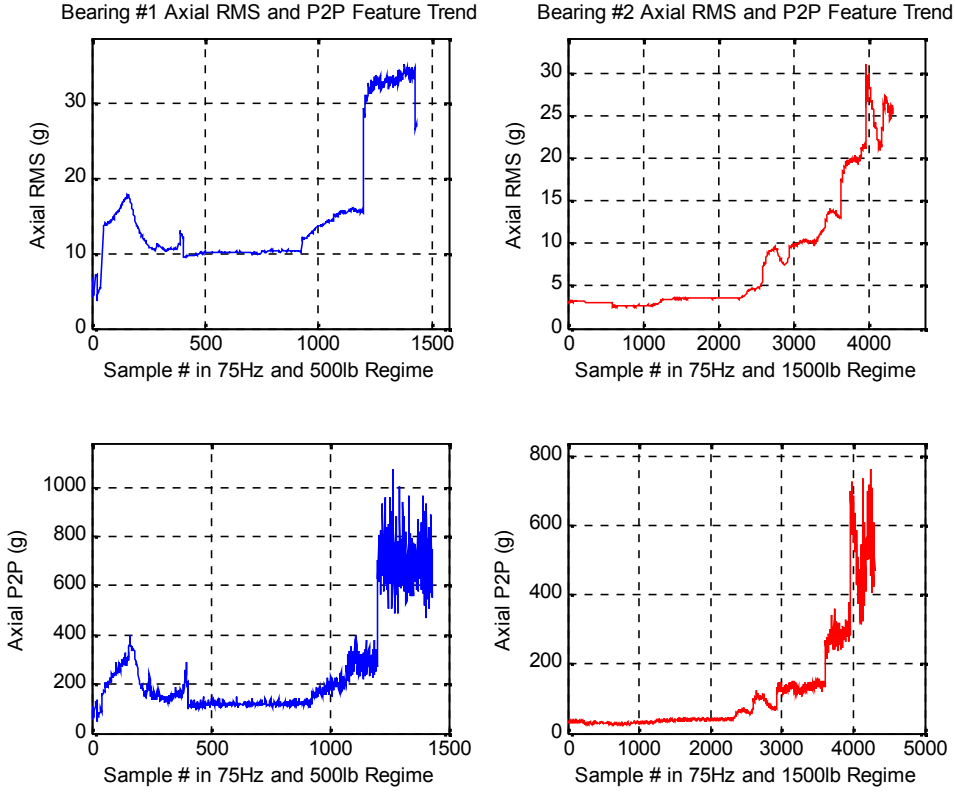


Fig. 10: Feature Trend in Axial Vibration RMS and P2P

Both bearings exhibited an inner race spall and eventual failure; one would expect that this type of physical defect would case an increase in energy around the ball pass inner race

and its first harmonic. The trend in the axial vibration envelope BPFI and 2X BPFI is shown in Fig. 11 for both bearings. Bearing #1 has a very clear increasing trend for both the BPFI and 2X BPFI features. The initial sharp rise in the BPFI and 2X BPFI features for Bearing #1 is when an inner race spall was first observed; however, the increasing trend does not occur until later during the progression test. The trend for Bearing #2 for the BPFI and 2X BPFI envelope features do not show a monotonic increasing trend, but at certain periods near the end of the test, these features exhibit much larger values than normal.

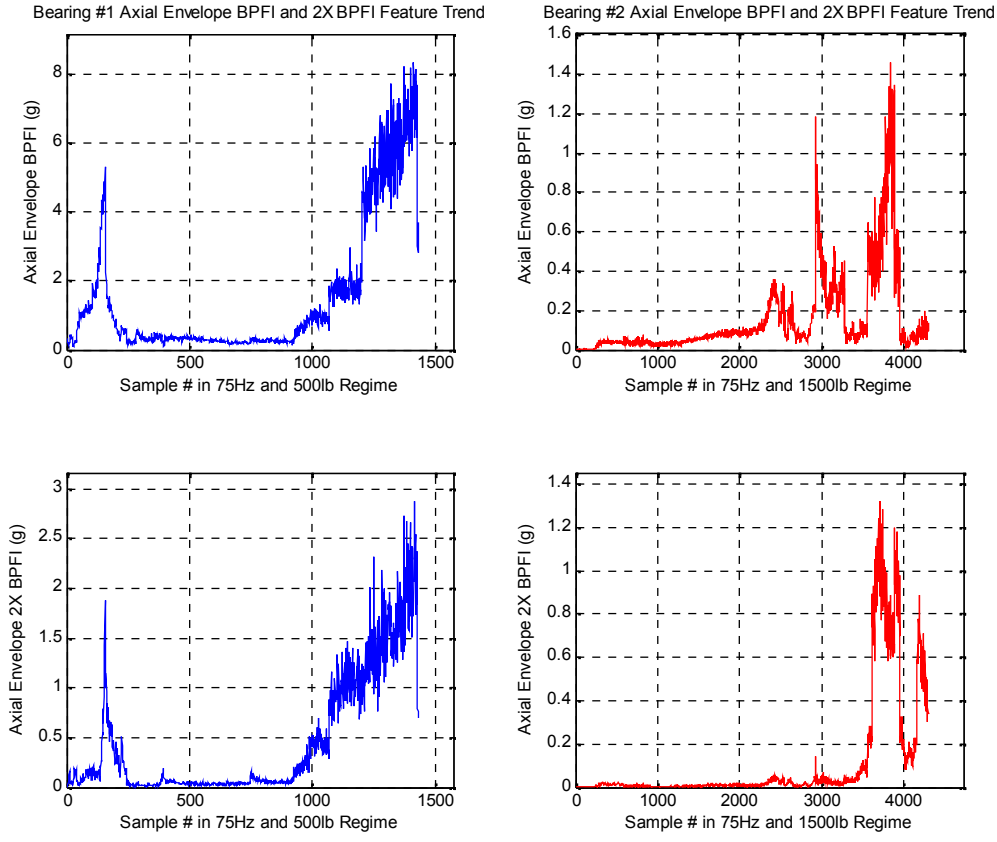


Fig. 11: Feature Trend in Axial Vibration Envelope BPFI and 2X BPFI

4.2 Feature Selection

Although visual examination of features can be used as an initial evaluation, it becomes quite difficult to visually examine all the potential vibration features that were extracted from the signal, given that this comprised of over 130 features. The initial plotting of a few of the key time domain and envelope fault frequency features shown previously highlights that a noticeable trend is prevalent in both data sets. The peak-to-peak and RMS features offered more promise for the second bearing data set, while the envelope BPFI features provided a monotonic trend for the first data set. There is value in determining other potential indicators in the remaining feature set. A method to rank the merits of the indicators is the objective of the feature selection routine. The literature in the area of feature selection is quite comprehensive and is usually divided into two categories—wrapper method and filter methods. Wrapper methods iteratively select the appropriate set of features by basing the performing on the output from a classification algorithm. This particular method requires selecting a discriminate method or algorithm prior to doing the feature selection routine [23]. The use of a wrapper method is not

entirely suited for this application, since the merits of the features are not based on distinguishing a normal from a degraded condition, but on showing a trend during the progression of the bearing until failure.

Filter methods do not require a classification or discriminate algorithm to be selected a priori, but instead rank the features based on some defined metric. The use of fishier criterion or correlation with certain output variables are some of the more common metrics used for ranking the merits of features [24]. For this particular application, the correlation metric was used, in that the ideal feature would show a high correlation with operating time from initial bearing spall until failure. This particular feature ranking was done for both run to failure data sets and the top 20 features that exhibited the most correlation with operating time are provided in Table 3. A quick observation of the feature selection results highlight that the features related to the envelope spectrum and in particular 2X BPFI envelope feature are high ranking for the data set for Bearing #1. However, time indicators such as variance, peak-to-peak, and RMS appear to offer the most insight into the failure progression for Bearing #2. Using the top-ranked features for each respective bearing data set would produce results that show a noticeable health trend over time; however, it was decided to use the top-ranked features for Bearing #2 to see if a more general set of indicators could be applied to both data sets.

Table 3: Feature Selection Ranking Results

	Top 20 Ranked Features for Bearing #1	Top 20 Ranked Features for Bearing #2
1	Axial 2X BPFI Envelope	Radial Variance LowPass
2	Axial Rolling Envelope	Axial Peak to Peak
3	Axial 2X BSF Envelope	Residual Axial Peak to Peak
4	Axial BSF Envelope	Radial Variance
5	Axial 2X BPFO Envelope	Residual Axial RMS
6	Axial Peak to Peak Envelope	Radial RMS LowPass
7	Axial BPFO Envelope	Radial RMS
8	TSA Axial 2X Peak	Axial RMS Peak to Peak
9	Axial Variance Envelope	Radial RMS Peak to Peak
10	Axial 2X Rolle Envelope	Residual Radial Peak to Peak
11	Axial BPFI Envelope	Radial RMS TSA
12	Axial 2X BPFI Envelope Normalized	Residual Radial RMS
13	Axial 2X FTF Envelope	Radial Variance TSA
14	Axial Variance TSA	Residual Radial Variance
15	Axial FTF Envelope	Radial Peak to Peak
16	Residual Axial Variance	Axial Crest Factor
17	TSA Axial 4X Peak	Radial Peak to Peak LowPass
18	Axial Variance	Axial RMS Envelope
19	Axial RMS TSA	Residual Axial Kurtosis
20	Axial Peak to Peak	Axial Kurtosis TSA

4.3 Health Assessment Method

The use of a single vibration indicator might not be sufficient for characterizing the bearing condition over time, in that a combined health indicator based on multiple features might provide a more robust indicator. For example, the bearing envelope analysis is known to provide good results when the bearing exhibits a localized point defect spall; however, the performance of this particular method is less promising when the defect area is more evenly spread [25]. It is unlikely that the nature of the spall is known beforehand or will remain constant over the progression of the bearing fault. Using multiple features allows one to include features that are suited for a point defect and a distributed fault to be included in the health assessment calculation.

The use of a distance-based metric is particularly suitable for combining multiple vibration indicators into a single health value; one particular advantage is that weighting of the individual features is not necessary for performing a distance-based calculation. There are a variety of distance metrics used in the literature, such as Mahalonbis distance, T-square, and Euclidean distance [26]. Considering the amount of noise and variance associated with the vibration features in this data set, it was decided to select a particular distance measure that would be less susceptible to this variation and noise. Neural networks for classification and other uses perform adequately with noise and variance in the features. Considering that the self-organizing map is a type of neural network that can also be used for performing a distance-based metric, this method was particularly suitable for this application. Also, in the work by Qui et al [27], the self-organizing map had previous success in assessing the health of rolling element bearings.

The mathematics behind the self-organizing map are only discussed within the context of its application for health monitoring, and the interested reader can find more detailed text on this particular algorithm [28]. The procedure for assessing the health using the self-organizing map is outline as follows:

1. Train the self-organizing map with the baseline vibration features selected by the feature selection routine.

2. For the currently monitored component, extract the selected vibration features and present this feature vector to the trained health map.

3. Find the best matching unit (BMU) between the test feature vector and the trained health map. The BMU is the node on the trained health map that is most similar to the test feature vector.

4. Calculate the minimum quantization error.

The equation for calculating the minimum quantization error is provided in Eqn 13, where MQE is the minimum quantization error, V is the test feature vector from the currently monitored component, and W_{BMU} is the BMU on the trained health map. Essentially, this calculation provides a measure of how far the condition of the currently monitored system or component is away from the normal or baseline region.

$$MQE = | V - W_{BMU} | \tag{13}$$

For this application, more than one baseline is needed for training since the run-to-failure testing was conducted in multiple operating regimes. The proposed approach for dealing with multiple operating regimes is shown in Fig. 12. Assigning the data into the appropriate operating regime or bin is the first step. For this application, grouping the data into different operating regime bins was rather straightforward since only two operating variables were considered—the radial load and the shaft speed. Ideally, one would want to have baseline training data in every potential operating regime; however, this is not entirely feasible. The more practical approach that is used for this study is to use the available training data and develop health models based on what data is available and also what are the most prevalent operating conditions that are seen in the field. This approach would imply that the health value is not calculated if a trained health model does not exist for that operating condition. For this application, the initial portion of the run-to failure data set was used for training the different health models. For Bearing #1 data set, there

were five main loading regimes and five trained health models, while the data set for Bearing #2 consisted of three main loading regimes, and, thus, three health models were used for that data set.



Fig. 12: Multi-Regime Health Assessment Approach

4.4 Health Assessment Results

The results for the self-organizing map health assessment method are presented with a health indicator value that is shown from the start of the test until the stopping of the test, when the bearing condition and vibration was deemed too severe to continue. The results for Bearing #1 are shown in Fig. 13; notice that the health value is relatively constant at the start of the test and has a step increase during the middle portion when a spall is initially formed. After the step increase, there is a noticeable increasing trend in the health value until the test is stopped; the end health value is approximately 10. The health value is an indication of how far the component is operating from the normal baseline condition, so a higher value is associated with a more degraded condition. There is some variation in the health value and also a spike in the health value prior to 800 operating minutes. If the trend in the health value is used for prediction, there are various algorithms that would be suitable for handling the spikes or noise in the health values.

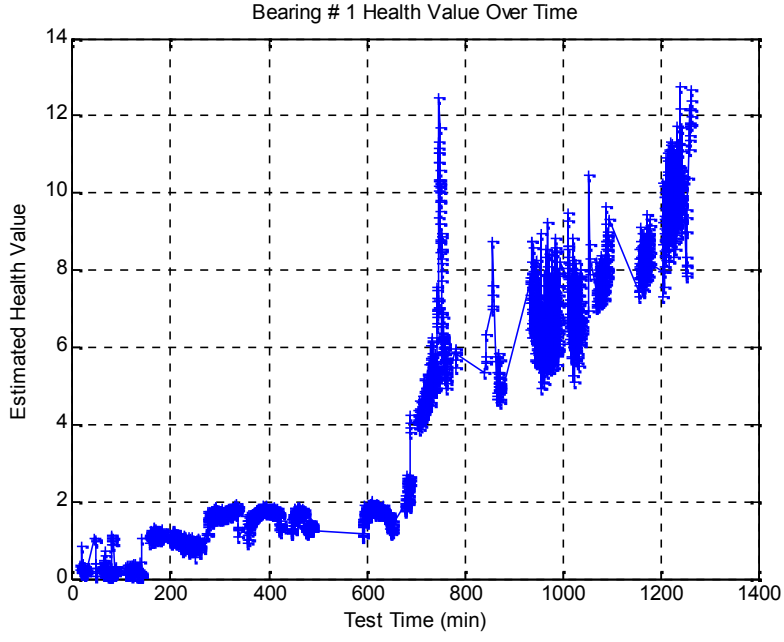


Fig. 13: Bearing #1 Health Value Trend Over Time

The health results for Bearing # 2 are provided in Fig. 14, and the health trend is not quite as clear for this particular data set. However, there is still an upward trend that is

noticeable after 1000 min of operating time and the end health value that is reached is also approximately 10. It is encouraging that the end health value is approximately 10 for both data sets; this is stating that the level of degradation for both bearings was approximately the same at the end of the test according to the health assessment method. A common end health value allows a failure threshold or failure zone to be established; this can be used to facilitate prediction methods, such as particle filtering or regression based methods.

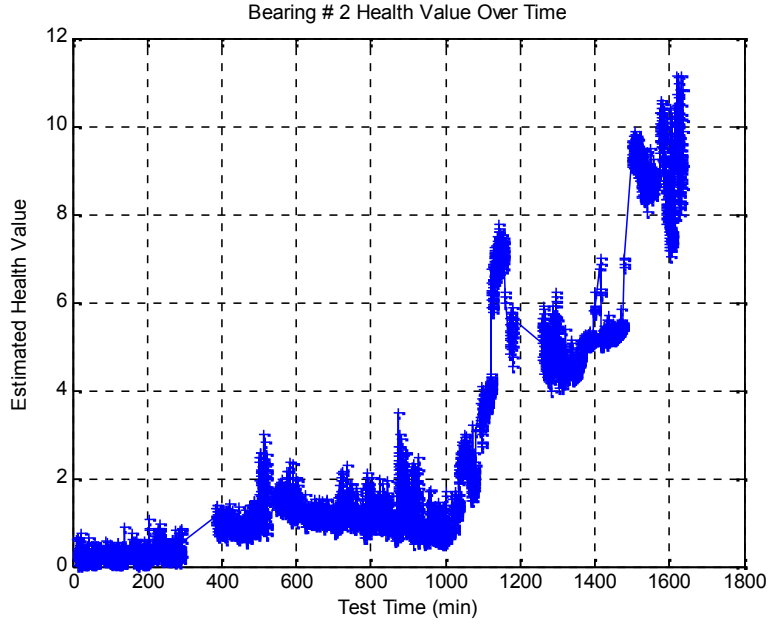


Fig. 14: Bearing #2 Health Value Trend over Time

5. Conclusions

This study focused on developing improved health and usage monitoring systems for helicopter drive-train components and, in particular, the oil-cooler bearing. At the foundation of health and usage monitoring system are the vibration signal processing and feature extraction techniques; this study reviewed many of the relevant techniques in order to compare traditional processing with more sophisticated processing methods. The results show that bearing envelope analysis and time domain statistical features appear the most promising for showing the progression of rolling element bearing failure. Using one or two features to monitor the health of rolling element bearings might not be sufficient. This is because the performance of individual features depends on the fault type, location, and whether the fault is distributed or closer to a point defect. For evaluation studies in which the potential set of features are quite large, it is perhaps logical to include a feature selection step in the overall methodology of developing health monitoring systems. Using a health assessment method that incorporates multiple bearing condition indicators appears to be a more robust option that can work for more general bearing failure modes. The results show an increasing health trend over time, with similar end health values for both bearing run-to-failure data sets. Future work would consider extending this current body of work and health assessment model to include prediction modeling and algorithms for estimating the remaining useful life of the oil-cooler bearings. A potential extension of this study would evaluate prediction approaches, including the use of particle filtering and regression-based prediction methods.

Acknowledgements

This work was funded under contract number W911NF-07-2-0075, and the experimental testing and data collection were performed by Impact Technologies, LLC. We would like to acknowledge Romano Patrick, Carl Byington, and other members of the Impact team for their collaboration in this research effort.

References

1. Samuel, P.D., Pines, D.J. (2005). A review of vibration-based techniques for helicopter transmission diagnostics, Journal of Sound and Vibration, Volume 282, pp. 475-508.

2. Kim, E.Y., Tan, A.C.C., Yang, B.S., Kosse, V. (2007). Experimental Study on Condition Monitoring of Low Speed Bearings: Time Domain Analysis, Proceedings of the 5th Australasian Congress on Applied Mechanics, ACAM 2007.

3. Qui, Hai, Luo, H., Eklund, N. (2009). On-Board Bearing Prognostics In Aircraft Engine: Enveloping Analysis or FFT, AFRL-RX-WP-TP-2009-4141.

4. McFadden, P.D., Smith, J.D. (1984). Vibration Monitoring of Rolling Element Bearings by High Frequency Resonance Technique – A Review, Tribology International, Volume 77, pp. 3-10.

5. Forrester, B.D. (1996). Advanced Vibration Analysis Techniques for Fault Detection and Diagnosis in Geared Transmission Systems, PhD Thesis, Swinburne University of Technology, Australia.

6. Peng, Z. K., Tse, P.W., Chu, F.L. (2005). A comparison study of improved Hilbert-Huang transform and wavelet transform: Application to fault diagnosis for rolling bearing,

7. Khatri, H., Ranney, K., Tom, K., Del Rosario, R. (2008). New features for Diagnosis and Prognosis of Systems Based on Empirical Mode Decomposition, Proceedings of the 2008 International Conference on Prognostics and Health Management.

8. Decker, H.J., Lewicki, D.G., (2003). Spiral Bevel Pinion Crack Detection in a Helicopter Gearbox, ARL-TR-2958, U.S Army Research Laboratory, NASA Lewis.

9. Vecer, P., Kreidl, M., Smid, R., (2005). Condition Indicators for Gearbox Condition Monitoring Systems, Acata Polytechnica Volume 45, No. 6.

10. Sawalhi, N., (2007). Diagnostics, prognostics, and fault simulation for rolling element bearings, PhD Dissertation, University of New South Wales, Sydney, Australia.

11. Thompson, J.K., Tree, D.R. (1980). Leakage Error in Fast Fourier Analysis, Journal of Sound and Vibration, Volume 71 (4), pp. 531-544

12. Harris, F.J. (1978). On the Use of Windows for Harmonic Analysis with the Discrete Fourier Transform, Proceedings of the IEEE, Volume 66 (1), pp. 51-83.

13. Howard ,I. (1994). A review of rolling element bearing vibration: detection, diagnosis, and prognosis, DSTO-RR-0013, Airframes and Engines Division.

14. Bechhoefer, E., Menon, P. (2009). Bearing Envelope Analysis Window Selection, Annual Conference of the Prognostics and Health Management Society 2009

15. Sawalhi, N., Randall, B. (2004). The application of Spectral Kurtosis to Bearing Diagnostics, Proceedings of Acoustics 2004, pp. 393-398.

16. Johansson, M. (1999). The Hilbert Transform, Master's Thesis, Vaxjo University, Vaxjo, Sweden.

17. Decker, H.J., Lewicki, D.G., (2003). Spiral Bevel Pinion Crack Detection in a Helicopter Gearbox, ARL-TR-2958, U.S Army Research Laboratory, NASA Lewis.

18. Luo, H., Qui, H., Ghanime, G., Hirz, M., Merwe, G.V.D. (2010). Synthesized Synchronous Sampling Technique for Differential Bearing Damage Detection, Journal of Engineering for Gas Turbines and Power, Volume 132 (7).

19. Decker, H.J., Zakrajsek, J.J. (1999). Comparison of Interpolation Methods as Applied to Time Synchronous Averaging, Proceeding of 53rd Meeting of the Society for Mechanical Failure Prevention Technology, NASA/TM -1999-209086, ARL-TR-1960, NASA Lewis Research Center

20. Blough, J.R. (1998). Improving the Analysis of Operating Data on Rotating Automotive Components, PhD Dissertation, University of Cincinnati, Cincinnati, Ohio

21. Antoni, J. (2006). The spectral kurtosis: a useful tool for characterizing nonstationary signals, Mechanical Systems and Signal Processing, Volume 20, pp. 282-307.

22. Antoni, J., Randall, R.B. (2006). The spectral kurtosis: application to the vibratory surveillance and diagnostics of rotating machines, Mechanical Systems and Signal Processing, Volume 20, pp 308-331.

23. Guyon, I., Elisseeff, A. (2003). An Introduction to variable and feature selection, The Journal of Machine Learning Research, Volume 3, pp. 1157-1182.

24. Hall, M.A. (2000). Correlation-Based Feature Selection for Discrete and Numeric Class Machine Learning, Proceedings of the 17th International Conference on Machine Learning, pp. 359-366

25. Steward, R.M. (1977). Some Useful Data Analysis Techniques for Gearbox Diagnostics, Institute of Sound and Vibration Research, Paper MHM/R/10/77.

26. Xiang, S., Nie, F., Zhang, C. (2008). Learning a Mahalanobis distance metric for data clustering and classification, Pattern Recognition, Volume 41, pp. 3600-3612

27. Qiu, H., Lee, J., Ling, J. Yu, G. (2003). Robust Performance Degradation Assessment Method for Enhanced Rolling Element Bearings Prognostics, Journal of Advanced Engineering Informatics, Vol. 17, pp. 127-140.

28. Kohonen T., Oja E., Simula O., Visa, A., Kangas J. (1996). Engineering application of the self-organizing map, Proceedings of the IEEE 84 (10) pp. 1358–1384.